Interactions between Organized, Surface-Confined Monolayers and Liquid-Phase Probe Molecules. 4. Synthesis and Characterization of Nanoporous Molecular Assemblies: Mechanism of Probe Penetration

Orawon Chailapakul and Richard M. Crooks*

*Department of Chemistry, Texas A&M University, College Station, Texas 77843-3255*

We report a detailed study of the physical and chemical properties of nanoporous, organomercaptan, self-assembled monolayers (SAMs). The present work expands upon our previous finding that two-component SAMs can serve as primitive models for studying molecular recognition phenomena. The monolayers self-assemble from solution-phase mixtures of two organomercaptans. One of these, which we call the framework component, is an *n*-alkanethiol (Au/HS(CH$_2$)$_{15}$CH$_3$) about 25 Å thick. The other is a much shorter organomercaptan (Au/HS(C$_6$H$_4$)OH), which we call the template, that induces defects within the much longer, kelp-forest-like framework. The number density of the templates on the metal surface is controlled by the template concentration in the ethanol solution from which it self-assembles and the total time allotted for self-assembly. Under the conditions used in this study the defects induced by the templates are of molecular dimensions and present at a number density of about 10^9/μm^2. The synthesis of these defect structures is reproducible and the nanoporous films themselves are stable under a wide variety of conditions. We characterize the monolayers using electrochemical methods. For example, we expose the probes to single- and multicomponent mixtures of redox probe molecules (including: Ru-(NH$_3$)$_6$$^{3+}$, Fe(CN)$_6$$^{4-}$, Mo(CN)$_8$$^{4-}$, Fe(CN)$_4(bpy)^{2-}$, Fe(bpy)$_2(CN)_2$, and cytochrome *c*) that have different hydrated radii, ionic charges, and heterogeneous electron-transfer rate constants. Cyclic voltammetry reveals that the probes are selectively passed through the nanoporous SAMs depending upon their properties. For probes of similar dimensions, selectivity is most closely correlated to ionic charge, although other factors are also important. We also find that the extent of probe penetration, and therefore the pore structure, is determined by the type and concentration of the electrolyte.

Introduction

Molecular recognition is the selective binding of a probe molecule to a molecular receptor. This binding interaction often relies on both noncovalent intermolecular chemical interactions, such as hydrogen bonding or van der Waals forces, and steric compatibility, such as size or shape inclusion. At present, a detailed understanding of molecular recognition phenomena is hindered primarily by two experimental problems. First, in many natural systems the receptor is a large, flexible, and complex molecule with many potential binding sites, and as a result it is difficult to quantify the specific types and magnitudes of interactions that lead to probe binding. Second, there are only a few analytical methods that are sufficiently specific and sensitive that they can be used for studying individual molecular interactions in bound probe/receptor complexes. These and other difficulties associated with natural systems have resulted in the synthesis of simpler model receptors and characterization of their interactions with probe molecules.[1-3]

Our studies of molecular recognition phenomena are based on the concept illustrated in Chart 1. The basic chemical building blocks are model organic surfaces consisting of self-assembled monolayers (SAMs) of organomercaptans.[4,5] It has previously been shown that *n*-alkanethiols spontaneously adsorb to Au from dilute solutions of ethanol and other nonaqueous solvents and

Chart 1
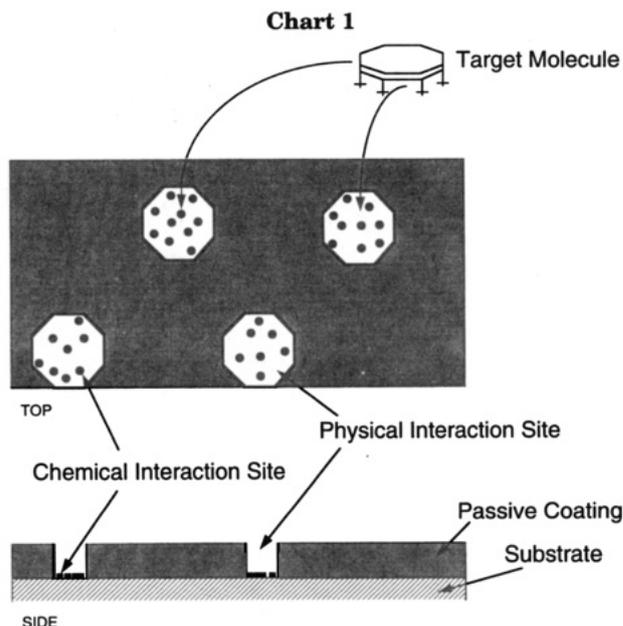
that the resulting SAMs assume a close-packed ($\sqrt{3}\times\sqrt{3}$)-R30° overlayer ($c(4 \times 2)$ unit cell) structure on Au(111) and other textured Au surfaces.[6] Spectroscopic studies indicate that monolayers formed from short organomercaptans are more disordered than those formed from longer-chain molecules, but their surface concentrations are roughly the same. The best *n*-alkanethiol monolayers contain surprisingly few adventitious defect sites, even when prepared on ill-defined substrates,[7-9] and most

---

(1) Wulff, G. In *Polymeric Reagents and Catalysts*; Fort, W. T., Ed.; ACS Symposium Series 308; American Chemical Society: Washington, DC, 1986; pp 186–230, and references therein.

(2) Lehn, J.-M. *Angew. Chem., Int. Ed. Engl.* **1990**, *29*, 1304.

(3) Rebek, J. J. *Acc. Chem. Res.* **1990**, *23*, 399.

(4) Nuzzo, R. G.; Allara, D. L. *J. Am. Chem. Soc.* **1983**, *105*, 4481.

(5) Dubois, L. H.; Nuzzo, R. G. *Annu. Rev. Phys. Chem.* **1992**, *43*, 437, and references therein.

(6) Pourier, G. E.; Tarlov, M. J. *Langmuir* **1994**, *9*, 2853.

(7) Chailapakul, O.; Crooks, R. M. *Langmuir* **1993**, *9*, 884.

(8) Chidsey, C. E. D.; Loiacono, D. N. *Langmuir* **1990**, *6*, 682.

SAMs are quite robust in aqueous solutions and vapor-phase ambients.

As in all natural and synthetic approaches to molecular recognition, interactions in the surface-confined systems described here are promoted at the ambient/receptor interface through both chemical and physical interactions (Chart 1). To simplify the analysis of these systems, we thought it would be advantageous to try to separate monolayer/molecule interaction phenomena into two distinct problems: one relating to purely chemical interactions, such as hydrogen bonding, and the other relating only to physical interactions, such as size exclusion; however, we have found that it is not feasible at present to achieve complete segregation of these two effects. In this paper, we focus primarily on physical interactions, although we will show that even under conditions where we anticipated observing size-exclusion-based molecular discrimination, chemical interactions dominate. We have previously discussed our efforts to better understand molecular recognition based primarily on chemical interactions in a different series of papers.[10-21]

The present work expands upon our previous finding that two-component SAMs can serve as primitive models for studying molecular recognition phenomena.[7] These nanoporous organic films are prepared from solution-phase mixtures of two organomercaptans. One of these, which we call the framework component, is an *n*-alkanethiol about 25 Å thick. The other is a much shorter organomercaptan, which we call the template, that induces defects within the much longer, kelp-forest-like framework. The number density of the templates on the metal surface is controlled by the template concentration in the ethanol solution, relative to the framework concentration, from which it self-assembles, and the total time allotted for self-assembly. Under certain conditions the defects induced by the templates are of molecular dimensions. The synthesis of these defect structures is reproducible and the nanoporous films themselves are stable under a wide variety of conditions.

To achieve our primary goal of understanding physical recognition behavior at the molecular level, it is important to address the following five questions: (1) how stable are template-induced defect sites; (2) what part do chemical interactions play at these "purely" physical interaction sites; (3) is the environment within the template-induced pockets hydrophilic or hydrophobic when the membranes are immersed in aqueous media; (4) can these structures be directly visualized and, if so, what is the geometrical relationship between the template molecules and the defect sites they define; (5) in what form do redox probe molecules enter the pores: do hydrated ions shed their hydration spheres as is often observed in bulk-phase host–guest chemistry? Here we begin to address the first three of these questions, and in future reports we hope to provide additional insight into these fascinating nanostructures.

We characterize nanoporous films using electrochemical methods. The framework portion of the monolayer is sufficiently thick that it effectively blocks electron transfer between the underlying electrode surface and solution-phase redox probe molecules. However, probe molecules that have the right combination of physical and chemical characteristics can penetrate the framework in the vicinity of template-induced defect sites and exchange electrons with the underlying Au electrode surface. The shape of the resulting cyclic voltammogram can be related to the size and number density of defects within the film. Our key finding is that only molecules with the right combination of hydrated radius and ionic charge can penetrate the framework; for molecules of similar size and shape, we find that charge is the principal factor that controls penetration.

In this paper we continue and expand our previous study by deploying a more extensive array of probe molecules, including: $Ru(NH_3)_6^{3+/2+}$, $Fe(CN)_6^{4-/3-}$, $Mo(CN)_8^{4-/3-}$, $Fe(bpy)_4(CN)_2^{2-/1-}$, $Fe(bpy)_2(CN)_2^{0/+}$, and cytochrome *c*. Our results indicate that for identical nanoporous films, different cyclic voltammetric signatures result for these redox probe molecules. Moreover, the type and concentration of supporting electrolyte also influence the extent of probe penetration. Finally, we show that these modified electrodes are capable of discriminating between different probe molecules in binary mixtures.

We[7] and others[22-33] have previously shown that the fractional surface coverage of defect sites in SAMs can be reproducibly varied by changing the relative concentrations of the template and framework molecules in the solution from which the composite monolayer assembles. For example, Whitesides' results for mixtures of short hydroxyl-terminated organomercaptans and longer *n*-alkanethiols, which are similar to the systems we have chosen to study, indicate the following: (1) mixed monolayers are inherently more disordered than single-component monolayers; (2) the monolayers consist of two regions: close to the Au surface there is some degree of ordering, but on the outer surface the monolayers are disordered; (3) longer organomercaptans preferentially adsorb to Au surfaces; (4) under certain conditions phase segregation occurs on a microscopic length scale; (5) the surface concentration of each constituent is related to the solution concentration, but this correlation cannot be

(9) Creager, S. E.; Hockett, L. A.; Rowe, G. K. *Langmuir* **1992**, *8*, 854.

(10) Sun, L.; Jonhson, B.; Wade, T.; Crooks, R. M. *J. Phys. Chem.* **1990**, *94*, 8869.

(11) Thomas, R. C.; Sun, L.; Ricco, A. J.; Crooks, R. M. *Langmuir* **1991**, *7*, 620.

(12) Sun, L.; Thomas, R. C.; Crooks, R. M.; Ricco, A. J. *J. Am. Chem. Soc.* **1991**, *113*, 8550.

(13) Sun, L.; Kepley, L. J.; Crooks, R. M. *Langmuir* **1992**, *8*, 2101.

(14) Kepley, L. J.; Crooks, R. M.; Ricco, A. J. *Anal. Chem.* **1992**, *64*, 3191.

(15) Bryant, M. A.; Crooks, R. M. *Langmuir* **1993**, *9*, 388.

(16) Xu, C.; Sun, L.; Kepley, L. J.; Crooks, R. M. *Anal. Chem.* **1993**, *65*, 2102.

(17) Chailapakul, O.; Sun, L.; Xu, C.; Crooks, R. M. *J. Am. Chem. Soc.* **1993**, *115*, 12459.

(18) Thomas, R. C.; Tangyunyong, P.; Houston, J. E.; Michalske, T. A.; Crooks, R. M. *J. Phys. Chem.* **1994**, *98*, 4493.

(19) Ricco, A. J.; Crooks, R. M.; Xu, C.; Allred, R. E. In *Interfacial Design and Chemical Sensing*; Mallouk, T. E.; Harrison, D. J., Eds.; ACS Symposium Series 561; American Chemical Society: Washington, DC, 1994; Chapter 23.

(20) Crooks, R. M.; Chailapakul, O.; Ross, C. B.; Sun, L.; Schoer, J. K. In *Interfacial Design and Chemical Sensing*; Mallouk, T. E., Harrison, D. J., Eds.; ACS Symposium Series 561; American Chemical Society: Washington, DC, 1994; Chapter 10.

(21) Crooks, R. M.; Sun, L.; Xu, C.; Hill, S. L.; Ricco, A. J. *Spectroscopy* **1993**, *8*, 28.

(22) Bain, C. D.; Whitesides, G. M. *J. Am. Chem. Soc.* **1988**, *93*, 3665.

(23) Bain, C. D.; Whitesides, G. M. *J. Am. Chem. Soc.* **1988**, *110*, 6560.

(24) Bain, C. D.; Whitesides, G. M. *Science* **1988**, *240*, 62.

(25) Bain, C. D.; Whitesides, G. M. *J. Am. Chem. Soc.* **1989**, *111*, 7155.

(26) Bain, C. D.; Whitesides, G. M. *J. Am. Chem. Soc.* **1989**, *111*, 7164.

(27) Bain, C. D.; Whitesides, G. M. *Angew. Chem., Int. Ed. Engl.* **1989**, *28*, 506.

(28) Whitesides, G. M.; Laibinis, P. E. *Langmuir* **1990**, *6*, 87.

(29) Stranick, S. J.; Parikh, A. N.; Tao, Y. T.; Allara, D. A.; Wiess, P. A. *J. Phys. Chem.* **1994**, *98*, 763.

(30) Laibinis, P. E.; Fox, M. A.; Folkers, J. P.; Whitesides, G. M. *Langmuir* **1991**, *7*, 3167.

(31) Folkers, J. P.; Laibinis, P. E.; Whitesides, G. M.; Deutsch, J. *J. Phys. Chem.* **1994**, *98*, 563.

(32) Kim, J.-H.; Cotton, T. M.; Uphaus, R. A. *J. Phys. Chem.* **1988**, *92*, 5575.

(33) Sagiv, J. *J. Am. Chem. Soc.* **1980**, *102*, 92.

predicted and is time dependent.[34] A very recent study reveals that, in some cases, the solution concentrations of two thiols are in equilibrium with the surface and that nanometer-scale phase segregation occurs on the surface.[29] In this study, scanning tunneling microscopy (STM) revealed that single-molecule phase domains were rather commonplace on the surface. This finding confirms our indirect observation of such domains[7] and adds credence to the model we propose here.

Research predating our own studies has shown that template-induced recognition sites can selectively readsorb the original template, but the more fundamental issue of how this happens at the molecular level has not been directly addressed for monolayer systems.[35–41] Important mechanistic information of this type is absent for two principal reasons: (1) lack of a structurally well-defined monolayer system in which to embed recognition sites; (2) inadequate analytical tools for directly visualizing nanometer-scale, template-induced physical recognition sites. We are presently in a position to begin addressing these two problems.

Sagiv was the first to consider using template molecules to perforate monolayer surfaces.[33,42,43] He used UV–vis and fluorescence spectroscopy to prove that monolayer surfaces formed by codeposition of alkylsilanes and template molecules yielded heterogeneous monolayers that preferentially readsorbed the template molecules in the presence of structurally related molecules. Kim *et al.* revisited this approach some years later and confirmed Sagiv's general findings using similar chemical systems and a surface-enhanced Raman spectroscopic probe.[32] Rubinstein *et al.* embedded molecular receptors within monolayers confined to Au substrate and showed they selectively absorbed metal ions.[44,45] In experiments conceptually similar to those discussed here, Bilewicz and Majda used Langmuir–Blodgett (L–B) methods to fabricate mixed-monolayers consisting of *n*-octadecanethiol framework molecules and ubiquinone "gate sites" (templates).[46,47] On the basis of electrochemical data, they proved that the ubiquinone gate sites provide electron-transfer pathways to the Au substrate and that the two-component L–B films act as ultramicroelectrode arrays. There have been several other related approaches for using monolayers, multilayers, and polymers, to direct size- and shape-based molecular recognition, but they all rely on the general principles discussed above.

Experimental Section

Chemicals. The following chemicals were used as received: $Fe(NH_4)_2(SO_4)_2 \cdot 6H_2O$, KCN, $CHCl_3$, C_5H_5N (Fisher); MoO_3, KNO_3, $(C_5H_4N)_2$ (2,2'-bipyridyl), K_2SO_4 (Aldrich); K_2HPO_4, KH_2PO_4 (Spectrum); cytochrome *c*, type VI from horse heart (99%, Sigma); KOH, KCl, KF, H_2SO_4, and H_2O_2 (J. T. Baker); KSCN (Mallinck-

rodt); C_2H_5OH (100%, Midwest grain products); $Ru(NH_3)_6Cl_3$ (Strem Chemicals). $HS(C_6H_4)OH$ (4-hydroxythiophenol, 4-HTP) was purified by vacuum sublimation before use. $HS(CH_2)_{15}CH_3$ ($C_{16}SH$) was purified by double distillation before use.

$Fe(bpy)_2(CN)_2 \cdot 3H_2O$ (dicyano-bis(2,2'-bipyridine)iron(II) trihydrate) was synthesized from $(C_5H_4N)_2$, $Fe(NH_4)_2(SO_4)_2 \cdot 6H_2O$, and KCN according to a literature procedure.[48–50] The complex was recrystallized from H_2SO_4 and was characterized by UV-vis and NMR spectroscopy and elemental analysis. Anal. Calcd for $Fe(bpy)_2(CN)_2 \cdot 3H_2O$: C, 55.71; H, 4.68; N, 17.71. Found: C, 55.0; H, 5.59; N, 17.32. The UV–vis spectroscopic data for $Fe(bpy)_2(CN)_2 \cdot 3H_2O$ in CH_3OH indicate absorptions at 248, 300, 366, and 556 nm (literature, 247, 300, 366, and 556 nm). ^1H NMR (CD_3OD) δ 9.64 (d, 1H), 8.43 (t, 2H), 8.03 (t, 1H), 7.91 (t, 1H), 7.59 (t, 1H), 7.3 (m, 2H). $Fe(bpy)_2(CN)_2^+$ was prepared by HNO_3 oxidation of the neutral compound.

$Fe(bpy)(CN)_4 \cdot 3H_2O$ (potassium tetracyanomono(2,2'-bipyridine)iron(II) trihydrate) was prepared by heating $Fe(bpy)_2(CN)_2 \cdot 3H_2O$ and KCN in a stream-bath for 24 h.[48–50] Evaporation of the dark orange, aqueous phase to a small volume with subsequent cooling yielded the crude product, which was recrystallized from a small quantity of water, filtered, and then dried in air at room temperature. Elemental analysis provided the following data. Anal. Calcd for $Fe(bpy)(CN)_4 \cdot 3H_2O$: C, 37.5; H, 3.12; N, 18.75. Found: C, 36.88; H, 2.79; N, 18.56. The UV-vis spectroscopic data for $Fe(bpy)(CN)_4 \cdot 3H_2O$ in CH_3OH indicate absorptions at 298, 375, and 544 nm (literature 298, 375, and 544 nm). ^1H NMR (D_2O) δ 9.17 (d, 1H), 8.06 (d, 1H), 7.78 (t, 1H), 7.32 (t, 1H).

$K_4Mo(CN)_8 \cdot 2H_2O$ (potassium octacyanomolybdate(IV) 2-hydrate) was synthesized from MoO_3, KSCN, C_5H_5N (pyridine), and KCN according to a literature method.[51] The dark amber crystals were precipitated from the concentrated solution in an ice bath. The crude product was purified in warm water using decolorizing charcoal, and a golden-yellow crystalline solid was formed by precipitation with CH_3CH_2OH. The crystals were collected, washed with alcohol, and dried under reduced pressure. The identity of the compound was confirmed by electrochemical and spectroscopic analyses.

Substrate Preparation. Prior to the experiments discussed later, the Au substrates were subjected to an extensive cleaning and annealing procedure, which greatly increases the Au(111) texture of the foils. Before each individual experiment a less extensive protocol was used to remove organic material from the electrode surfaces without damaging the underlying Au lattice.

The following procedure was applied to each substrate once prior to the experiments discussed herein. Au foil (0.1 mm thick, Aesar, 99.95%) was cut into 1 cm × 1 cm pieces with a narrow section extending out from one corner to make electrical contact.[52] The electrodes were placed in quartz holders and cleaned in a freshly prepared piranha solution (3:1 H_2SO_4:30% H_2O_2) for 5 min, rinsed extensively with water, and then dried under a stream of N_2. (**Caution:** piranha solution is a powerful oxidizing agent and reacts violently with organic compounds. It should be discarded immediately after use in a waste container with a loosely fitting lid.) The foil was etched in warm (50–70 °C) aqua regia (3:1 concentrated HCl:HNO_3) for 15 s, rinsed with water, and again dried under N_2. (**Caution:** aqua regia is a powerful corrosive agent. It should be discarded immediately after use in an appropriate waste container.) The foil was transferred to a quartz tube and annealed in a calibrated Lindberg tube furnace (Model 55035) at 1030 °C for 5 h under a flowing (2 mL/min) Ar atmosphere. The Au foil was then cleaned cathodically for 10 min at a current density of 5 mA/cm^2 (all current densities are based on the area of both sides of the 1 cm × 1 cm Au foils) in a 3 M NaOH electrolyte solution (70–80 °C). The Au foil was rinsed thoroughly with water, soaked in 10 M HNO_3 for 1 min, rinsed again, and then anodically cleaned at a current density

(34) Folkers, J. P.; Laibinis, P. E.; Whitesides, G. M. *Langmuir* **1992**, *8*, 1330.

(35) Cao, G.; Hong, H.-G.; Mallouk, T. E. *Acc. Chem. Res.* **1992**, *25*, 420, and references therein.

(36) Jonhson, J. W.; Jacobson, A. J.; Butler, W. M.; Rosenthal, S. E.; Brody, J. E.; Lewandowski, J. T. *J. Am. Chem. Soc.* **1989**, *111*, 381.

(37) Cao, G.; Mallouk, T. E. *Inorg. Chem.* **1991**, *30*, 1434.

(38) Tabushi, I.; Kurihara, K.; Naka, K.; Yamamura, K.; Hatakeyama, H. *Tetrahedron Lett.* **1992**, *28*, 4299.

(39) Tao, U.-T.; Ho, Y.-H. *J. Chem. Soc., Chem. Commun.* **1988**, 417.

(40) Yamamura, K.; Hatakeyama, H.; Naka, K.; Tabushi, I.; Kurihara, K. *J. Chem. Soc., Chem. Commun.* **1988**, 79.

(41) Gould, S.; Meyer, T. J. *J. Am. Chem. Soc.* **1991**, *113*, 7442.

(42) Sagiv, J. *Isr. J. Chem.* **1979**, *18*, 346.

(43) Sagiv, J. *Isr. J. Chem.* **1979**, *18*, 339.

(44) Rubinstein, I.; Steinberg, S.; Tor, Y.; Shanzer, A.; Sagiv, J. *Nature* **1988**, *332*, 426.

(45) Steinberg, S.; Tor, Y.; Sabatani, E.; Rubinstein, I. *J. Am. Chem. Soc.* **1991**, *113*, 5176.

(46) Bilewicz, R.; Majda, M. *J. Am. Chem. Soc.* **1991**, *113*, 5464.

(47) Bilewicz, R.; Majda, M. *Langmuir* **1991**, *7*, 2794.

(48) Saji, T. Y.; Aoyagui, S. *J. Electroanal. Chem.* **1975**, *61*, 147.

(49) Schilt, A. A. *J. Am. Chem. Soc.* **1960**, *82*, 3000.

(50) Bryant, G. M.; Fergusson, J. E.; Powell, H. K. *J. Aust. J. Chem.* **1971**, *24*, 257.

(51) Furman, N. H.; Miller, C. O. *Inorg. Syn.* **1950**, *3*, 160.

(52) In ref 7, we incorrectly gave the electrode size as being 1 cm × 2 cm (however, this error did not affect any of the calculated results). In that work, as well as that discussed here, the electrodes areas are all 1 cm²/side.

of 5 mA/cm² for 10 min in a stirred 1 M H₂SO₄ solution at 25 °C. Finally, the Au foil was again thoroughly rinsed with water.

Anodic polishing of the Au foil was performed by placing the foil into a 1:1:2 solution of ethylene glycol, 100% ethanol, and 12 M HCl, respectively. The Au electrode was held at 2 V (current density = 0.05–0.1 A/cm²) for 1 min and then switched to 4.5 V (current density = 0.20–0.25 A/cm²) for 10 s. The Au foil was rinsed with water, cleaned in piranha solution for 1 min, soaked in a 1:1:2 solution of ethylene glycol, 100% ethanol, 12 M HCl solution for 10 s. Then the Au foil was rinsed with water, cleaned in piranha solution, and rinsed again prior to annealing a second time at 1030 °C for 5 h under flowing Ar. This procedure is similar to one used by Creager and co-workers,[9] and it leads to Au substrates that support *n*-alkanethiol SAMs that have very low defect densities.

Solutions containing a mole ratio of 4-HTP/C₁₆SH = 5 in ethanol (total organomercaptan concentration = 2 mM) were freshly prepared prior to soaking the electrodes. Before *each* surface modification, the Au electrodes were cleaned by dipping in freshly prepared piranha solution for 5 min, 6 M HCl for 10 s, and then piranha solution for 2 min. The Au electrodes were sometimes electrochemically cycled 2 or 3 times between 0 and +1.5 V in 0.1 M HClO₄ to eliminate oxides from the Au surfaces (the electrode was removed from the electrolyte solution at 0 V), which are introduced by the piranha cleaning step. However, we found that electrochemical oxide reduction did not result in an improvement in the passivating properties of the SAMs or in enhanced reproducibility; on the basis of XPS data not discussed here, we speculate that the organomercaptans themselves dissolve thin layers of Au oxides. Finally, the electrodes were rinsed with copious amounts of water followed with ethanol before immediately immersing them in the mixed organomercaptan solution for 36 h (unless otherwise indicated).

Electrochemical experiments were carried out in a single-compartment, three-electrode, glass cell containing a Ag/AgCl, NaCl (3 M) reference electrode (Bioanalytical Systems, Inc.) and a Pt-gauze counter electrode. Control experiments indicated that atmospheric oxygen did not interfere with the electrochemical results, so solutions were not degassed prior to use. All electrochemical experiments were performed with a Pine Instruments Model AFRDE4 bipotentiostat, and data were recorded on a Kipp and Zonen Model BD-90 X-Y recorder. The voltammograms in all figures were obtained in alphabetical sequence.

Results and Discussion

Two-Component Monolayer Formation Kinetics. The factors governing formation of two-component SAMs are not well understood at the present time. Three studies have been illuminating, however. Chidsey *et al.*[53] showed that when a mixed monolayer was exposed to a solution containing only one molecular component of the SAM, the fractional surface coverage of that species increased over time. On the basis of this experiment, they speculated that the initially formed monolayer contains defective regions (for example, tilt boundaries or substrate-induced defects). In their model, molecules in the vicinity of these defects are labile and can exchange with solution-phase organomercaptan molecules. The exchange process in these experiments was relatively fast during the first 2 days of incubation, but extended exposure failed to yield a solution-equilibrated substrate: a significant fraction of the original SAM was irreversibly bound. Rowe and Creager observed similar behavior.[54] In experiments conceptually linked to those discussed here, Whitesides *et al.* used contact-angle measurements to study the formation kinetics of two-component monolayers. The results of their studies, which were briefly discussed earlier, are in general agreement with Chidsey's.

In our previous study we incubated the Au substrates with the ethanolic solution of the framework and template
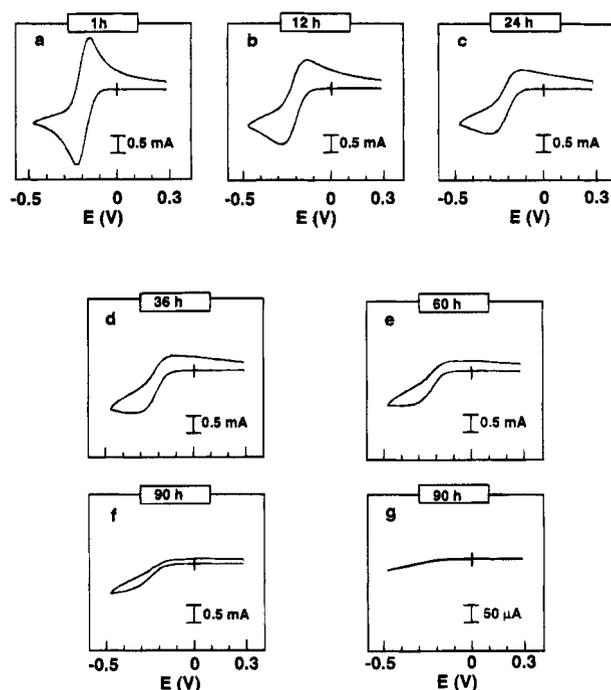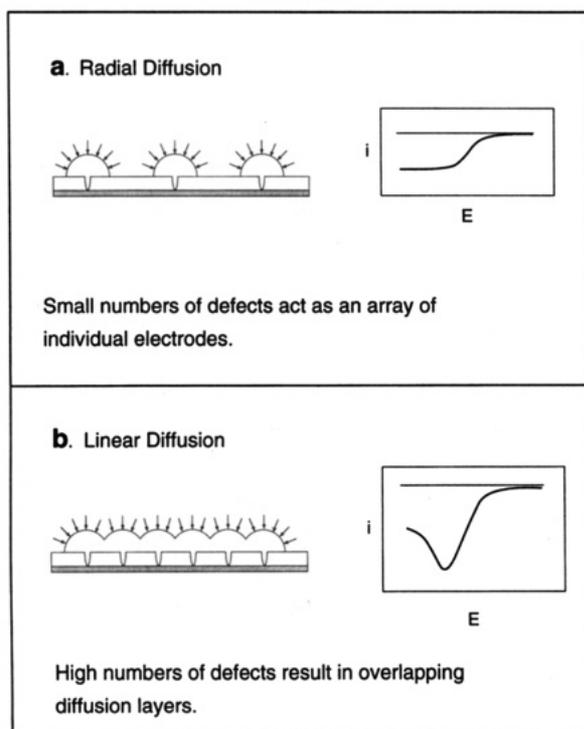
(53) Chidsey, C. E. D.; Bertozzi, C. R.; Putvinski, T. M.; Mujsce, A. M. *J. Am. Chem. Soc.* **1990,** *112,* 4301.
(54) Rowe, G. K.; Creager, S. E. *Langmuir* **1994,** *10,* 1186.

Figure 1. Cyclic voltammograms of 5 mM Ru(NH₃)₆³⁺ obtained using (a–f) nanoporous-SAM electrodes fabricated by immersing a Au surface in ethanol solutions containing a ratio of 4-HTP/C₁₆SH = 5 (2 mM total mercaptan concentration) for the time periods indicated in each frame. (g) Voltammogram of a Au surface modified with C₁₆SH only for 90 h. The data were obtained using a scan rate of 0.1 V/min in an aqueous electrolyte solution containing 1.0 M KCl. All data, except for part g, were obtained on the same electrode.

organomercaptans for at least 36 h. To determine the extent to which this set of conditions yields limiting behavior, we examined the cyclic voltammetry of modified electrodes as a function of their exposure time to the organomercaptan solution (Figure 1). We cleaned and annealed an Au foil electrode as described in the Experimental Section, and then it was immersed in an ethanolic organomercaptan solution containing a mole ratio of 4-HTP/C₁₆SH = 5 for 1 h. We removed the electrode, rinsed it thoroughly with gently flowing ethanol and water, and then placed it into an aqueous electrolyte solution containing 1.0 M KCl and 5 mM Ru(NH₃)₆³⁺ for electrochemical analysis. We chose 4-HTP/C₁₆SH = 5 because previous studies indicated this ratio results in a convenient fractional surface concentration of molecule-sized defects.[7] The voltammogram that results from the 1 h soaking period (Figure 1a) is essentially identical to that obtained at a naked Au electrode, which indicates the nanoporous monolayer contains many defect sites through which Ru-(NH₃)₆³⁺ can penetrate. These defects may result from either a poorly formed SAM composed of primarily C₁₆SH or a SAM containing many 4-HTP-induced defect sites. Since SAMs formed for 1 h in a pure C₁₆SH solution yield electrodes that largely passivate electron transfer, we believe initial contact between the deposition solution and the substrate results in a high surface concentration of 4-HTP, which permits electron transfer, and a comparatively small fractional coverage of C₁₆SH, which blocks electron transfer. The result is a surface that contains many small electrochemically active regions that have overlapping diffusion layers. This configuration, which is illustrated in part b of Chart 2, yields a cyclic

Chart 2

a. Radial Diffusion

Small numbers of defects act as an array of individual electrodes.

b. Linear Diffusion

High numbers of defects result in overlapping diffusion layers.

Figure 2. Cyclic voltammograms of 5 mM $Ru(NH_3)_6^{3+}$ as a function of scan rate. The electrolyte solution contained 1 M KCl. All data were obtained using a single electrode.

voltammetric signature very similar to that of a naked electrode or an electrode covered with a full monolayer of 4-HTP.[55]

After recording the data in Figure 1a, we removed the electrode from the $Ru(NH_3)_6^{3+}$ test solution, rinsed it with water and ethanol, and immersed the same electrode in the same 4-HTP/C_{16}SH = 5 solution for a total of 12 h. Again the electrode was removed, rinsed, and tested electrochemically to determine the relative defect density of the monolayer. We continued this procedure for a total of 2 weeks. Cyclic voltammetric data obtained during the first 90 h of this period are shown in Figure 1c−f.

The complete data set (Figure 1a−f) reveals a trend toward smaller defect densities and probably smaller defects as the modification time increases. The voltammetry is initially governed by linear diffusion (Figure 1a), but after a 12-h modification it appears to result more from mixed linear/radial diffusion (Figure 1b−d). Finally, the voltammetry is characteristic of nearly pure radial diffusion (Figure 1e,f), which is characteristic of that expected from an array of ultramicroelectrodes (UMEs) having sufficiently small dimensions and being sufficiently widely spaced that their diffusion layers do not overlap (Chart 2, part a). A simple calculation indicates that the latter condition obtains when the ratio of the average distance between electrode centers to their average diameters is greater than about 10.[56] We have previously shown that these electrodes are of molecular dimensions, so this simple analysis indicates the defects responsible for the voltammetry shown in Figure 1f could be spaced as closely as 10 nm, although they are actually much more widely spaced (*vide infra*).

To demonstrate that the 4-HTP template molecules are responsible for the Faradaic current shown in Figure 1a−f, we also show an example of the voltammetry that results from an electrode that was modified for 90 h in an ethanol solution containing only C_{16}SH (Figure 1g, note change
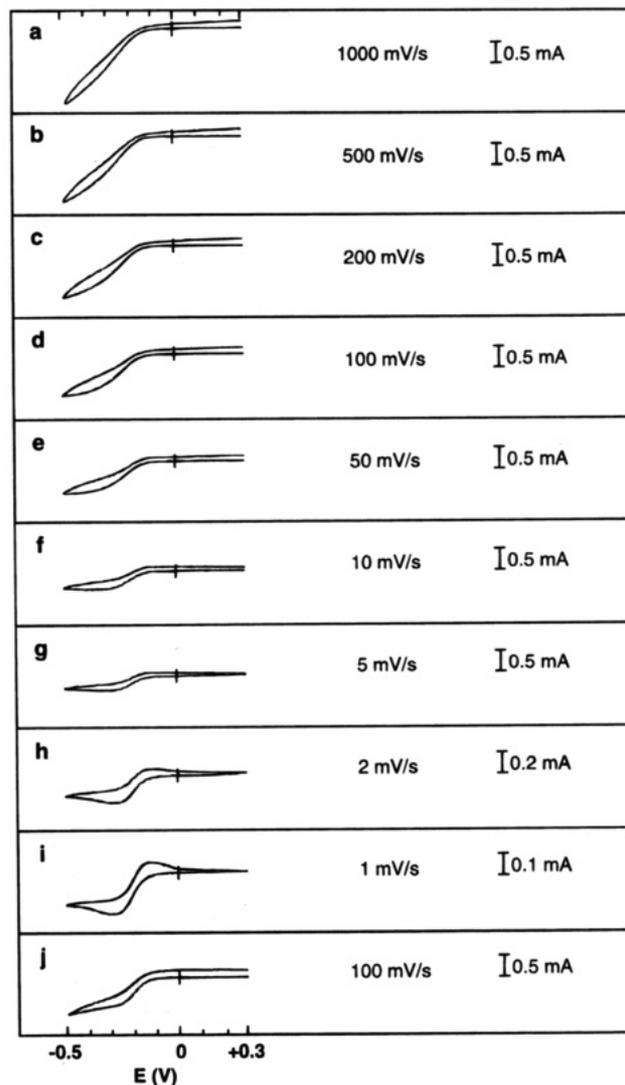
in current scale). This important experiment clearly demonstrates that the template molecules originally present in the soaking solution are resident on the Au surface and that they are responsible for the Faradaic electrochemical activity of the two-component-modified electrodes.

We were able to achieve a limiting concentration of template molecules within the SAMs: modification times ranging from 1−2 weeks yielded electrodes whose voltammograms are nearly identical and that had limiting currents indistinguishable (within the accuracy of the technique) from Figure 1f. However, at shorter times there is continuous exchange of the shorter template molecules for the more thermodynamically stable framework molecules during SAM formation. This result confirms earlier studies, which have shown that longer molecules compete more effectively for surface adsorption sites and that the SAM slowly achieves equilibrium with the solution.[22−27,30,31,34] We chose a soaking time of 36 h for the remaining studies reported here, since differences in the monolayer structure are not sensitive to small differences in soaking times after the first 24 h. More importantly, a 36-h soaking time yields reproducible nanoporous surfaces that have the most desirable distribution of template sites, which are stable for days in air and aqueous electrolyte solutions.

(55) Sabatani, E.; Rubinstein, I. *J. Phys. Chem.* **1987**, *91*, 6663.
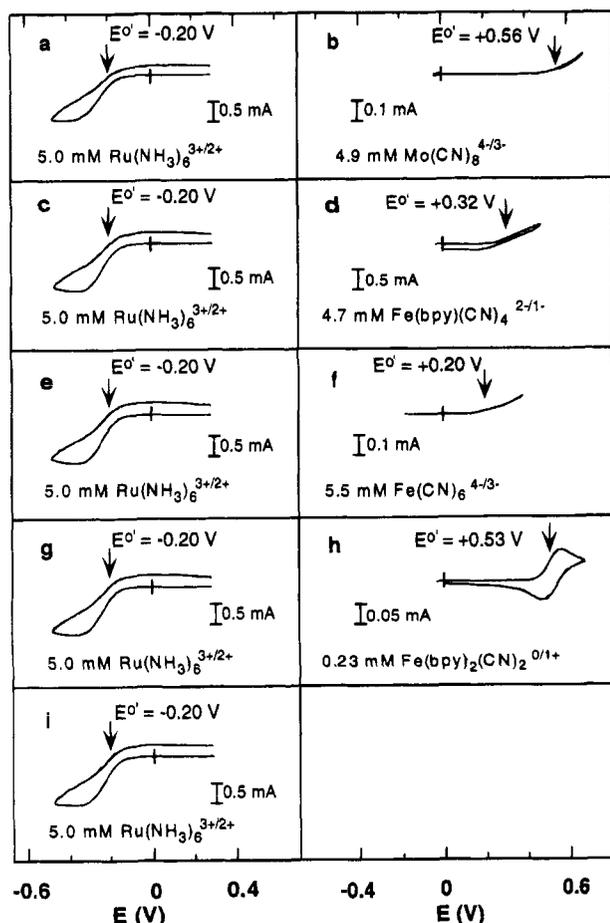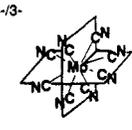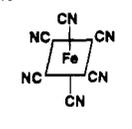(56) Bard, A. J.; Faulkner, L. R. In *Electrochemical Methods*; Wiley: New York, 1980; Chapter 6.
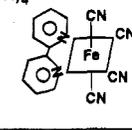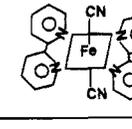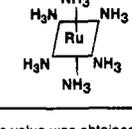
Figure 3. Cyclic voltammograms for nanoporous-SAM electrodes. The probe molecules, their concentrations, and their $E^{\circ\prime}$ values measured on naked electrodes are indicated in each frame. The aqueous electrolyte solution contained 0.2 M KF for the data on the right side of the figure and 1.0 M KCl for the data on the left. All voltammograms were recorded at 0.1 V/s. All data were obtained using a single electrode.

Figure 2 shows the scan rate dependence for the reduction and oxidation of a 5.0 mM $Ru(NH_3)_6^{3+}$ solution obtained at a nanoporous SAM prepared by immersion of a Au electrode in a 4-HTP/C_{16}SH = 5 solution for 36 h. There are two important results that we obtain from these data. First, between 5 and 100 mV/s, where the voltammetry is well behaved, the maximum current changes by only 60%. For pure radial diffusion, we would predict no change, while pure linear diffusion would result in a change of more than 400% over this range of scan rates. This suggests that the current is controlled primarily by radial diffusion.[57] Second, the shape of the voltammograms becomes more characteristic of linear diffusion at slower scan rates (Figure 2i). This observation serves to confirm our assertion that nanoporous SAMs are best characterized as an array of very small ultramicroelectrodes: a component of linear diffusion obtains because of overlapping diffusion layers at the slower scan rates. That is, at the slow scan rates there is a transition from the behavior illustrated in part a of Chart 2 to the behavior shown in part b.

Evaluation of Defect Structures. It is critical to quantitatively evaluate the size, number density, and distribution of template-induced defect sites on the electrode surface. We have pursued two approaches to this problem. The first, which should be the most

Chart 3

a   This value was obtained from: Otashima,K; Kotato, M.; Sugawara, M.; Umezawa, Y. *Anal. Chem.* **1993**, *65*, 927, and the diffusion coefficient was estimated to be 5.4x10⁻⁶ cm²/s at 25 °C from the Stokes-Einstein equation (see reference 65).

b   Hydrated diameter estimated from the diffusion coefficient at 25 °C and the Stokes-Einstein equation (see reference 65).

c   Same as (b) except at 22 °C.

straightforward to interpret, is based on direct observation of the pores by STM. However, this has turned out to be an extremely difficult analysis problem for several reasons.[20,58,59] Since the template-induced pores are sparsely distributed (about 10 defects/μm²),[7] only of molecular dimensions, and of low image contrast,[58] it is very difficult to locate them using STM and even more difficult to construct a statistically significant picture of their characteristics. Our approach to overcoming these problems involves etching the underlying Au substrate in dilute cyanide solutions in the vicinity of the defects while examining changes in topography by STM. This strategy increases the size and image contrast but results in loss of information about the size and shape of the original defects.

The second method for evaluating the characteristics of template-induced defects, which is the one we have chosen to exploit here, involves the use of electrochemical methods to evaluate interactions between the defect sites and probe molecules having different physical and chemical characteristics. By examining the voltammetry of the modified electrodes as a function of the size, ionic charge, molecular structure, and standard electron-transfer rate constant (k°) of the probe molecules, we can indirectly infer some information about the chemical and physical nature of the defect sites.

Figure 3 shows a series of voltammograms we obtained by using a single 4-HTP/C_{16}SH-coated electrode in the presence of the five different probe molecules illustrated in Chart 3. The voltammetry of all five probe molecules

(57) Wightman, R. M.; Wipf, D. O. In *Electroanalytical Chemistry*; Bard, A. J., Ed.; Dekker: New York, 1989; Vol. 15.

(58) Sun, L.; Crooks, R. M. *J. Electrochem. Soc.* **1991**, *138*, L25.
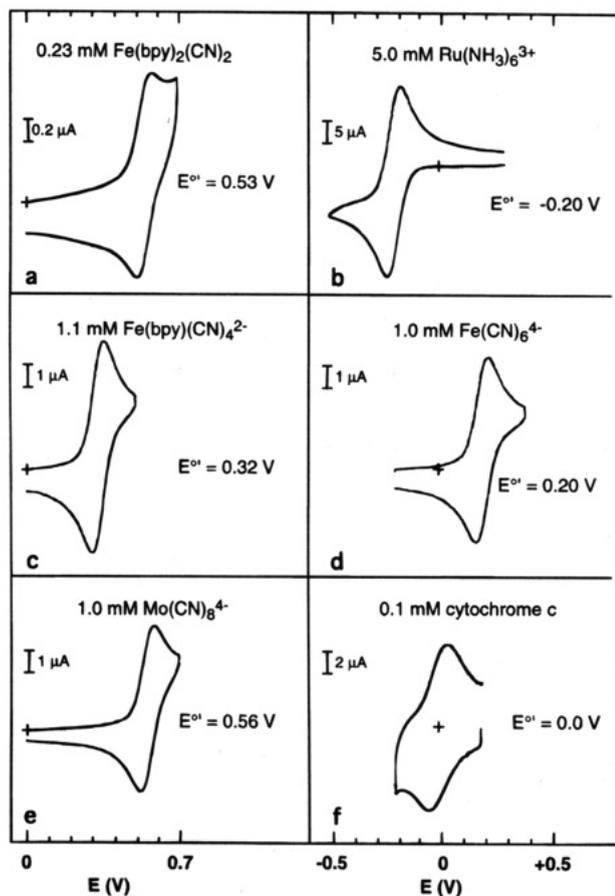(59) Sun, L.; Crooks, R. M. *Langmuir* **1993**, *9*, 1951.

Figure 4. Cyclic voltammetry of the probe molecules used in this study: (a–e) obtained on naked Au disk electrodes (area = 0.02 cm^2) in an aqueous 0.2 M KF electrolyte solution (except b, which was 1.0 M KCl) at a scan rate of 0.1 V/s. The concentration of the probe molecule is indicated in each frame. The data shown in (f) were obtained at a 1 cm × 1 cm Au flag electrode previously modified with a single monolayer of 4-hydroxythiophenol, which favors reversible voltammetry.[76] The electrolyte solution contained 0.1 M NaClO$_4$ + 20 mM pH = 7 aqueous phosphate buffer and the scan rate was 0.05 V/s. The measured $E^{\circ\prime}$ values, which were obtained by averaging the potentials corresponding to the peak anodic and cathodic currents, are indicated in each frame.

obtained at naked Au electrodes is shown in Figure 4. We selected these probes on the basis of their formal redox potential, which must be compatible with the stability limits of the SAM (roughly −0.5 to +0.7 V under the conditions used in this study), and because of their differing sizes, ionic charges, and k° values. When we examined the voltammetry of the probes at SAMs consisting of C$_{16}$-SH only, we observed a response much like that shown in Figure 1g, which is characterized by a background current less than 5% of the current observed at the perforated SAMs over the indicated potential range.

We ensured that the structure of the nanoporous SAMs did not change as a function of time or potential by periodically performing control experiments using Ru-(NH$_3$)$_6$$^{3+}$ as a standard probe molecule; we also followed this strategy in most of the remaining experiments. For example, in Figure 3, we obtained a voltammogram of Ru(NH$_3$)$_6$$^{3+}$ prior to every other voltammogram. The differences in the voltammetry from run to run are minimal as shown on the left side of the figure, which permits direct, qualitative comparison of the voltammetry of the other probe molecules and confirms the reproducibility and stability of the two-component SAMs.

Since we do not have good evidence for the structure of the defect sites, we somewhat arbitrarily postulate them

Chart 4
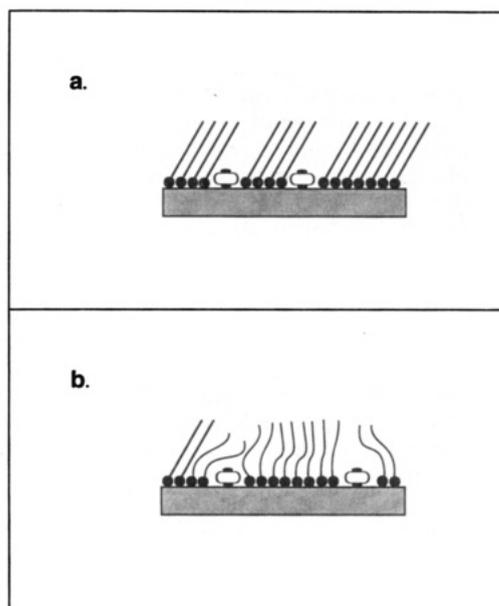
to be similar to those illustrated in Chart 4. One property of the defects is certain: their lateral size is on the order of molecular dimensions.[7] We also believe it is reasonable to assume that the defect sites possess a range of conformations: for example, some of them might permit closer approach of the probe molecules to the electrode surfaces than others.

If we assume that there is a range of structurally distinct defect sites that permit penetration of the probes to different distances of closest approach to the electrode surface, then k° should strongly affect the observed voltammetry. Probe molecules having larger k° values will be able to exchange electrons at defect sites that are not active for probes with small k° values, and more Faradaic current will be observed for the former. Since we are interested in synthesizing monolayers that respond to the chemical and physical characteristics of molecules rather than their intrinsic electron-transfer kinetics, we prefer a homogeneous distribution of defect site such as those in Chart 4, Part a.

The voltammetry in parts g and h of Figure 3 demonstrate that k° is not a dominant factor controlling molecular selectivity. The sigmoidal voltammogram shown in Figure 3g is characteristic of radial diffusion to defect sites whose diffusion layers do not overlap. This indicates that Ru-(NH$_3$)$_6$$^{3+}$ is only able to access small, widely spaced defect sites (Chart 2, part a). However, the voltammetry observed for Fe(bpy)$_2$(CN)$_2$ results from linear diffusion (Chart 2, part b), which arises from overlapping diffusion layers of pores that are significantly more closely packed than those probed by Ru(NH$_3$)$_6$$^{3+}$.[47,56,60,61] Since the same nanoporous electrode was used to obtain the data in parts g and h of Figure 3, we conclude that some defect sites that are accessible to Fe(bpy)$_2$(CN)$_2$ are not accessible to Ru(NH$_3$)$_6$$^{3+}$. This indicates a degree of molecular discrimination based on some property of the probes other than k°, since k° is larger for Ru(NH$_3$)$_6$$^{3+}$ ($k^\circ > 1$ cm/s)[46,62] than it is for Fe(bpy)$_2$(CN)$_2$ ($k^\circ = 0.63$ cm/s).[48] Indeed, the data suggest that ionic charge dominates transmonolayer mass transfer in this case since the hydrated radius of

(60) Amatore, C.; Savéant, J.-M.; Tessier, D. *J. Electroanal. Chem.* **1983**, *147*, 39.

(61) Cheng, I. F.; Martin, C. R. *Anal. Chem.* **1988**, *60*, 2163.

(62) Endicott, J. F.; Schroeder, R. R.; Chidester, D. H.; Ferrier, D. R. *J. Phys. Chem.* **1973**, *77*, 2579.

$Ru(NH_3)_6^{3+}$ at 22 °C (6.4 Å),[63,64] which we calculated from the Stokes–Einstein equation,[65] is smaller than that of $Fe(bpy)_2(CN)_2$ (11.4 Å).[48] Clearly, if discrimination was based solely on size exclusion, the larger $Fe(bpy)_2(CN)_2$ would be able to access fewer defect sites and a lower limiting current would result.

The importance of ionic charge to pore penetration is further underscored by comparing the voltammograms for $Mo(CN)_8^{4-}$, $Fe(CN)_6^{4-}$, $Fe(bpy)(CN)_4^{2-}$, and $Fe(bpy)_2$-$(CN)_2$ (Figure 3). All four of these probe molecules have about the same $k°$ value (the range is 0.15–0.63 cm/s),[48,66] but they show large differences in oxidation current (normalized for probe concentration) at $E^{o\prime}$ ($i_{E^{o\prime}}$), which we take as a good qualitative measure of effective pore penetration for molecules with similar $k°$ values. For this series of probe molecules, $i_{E^{o\prime}}$ is highest for the uncharged molecule, attains an intermediate value for the ion with charge 2−, and is smallest for the two ions with charge 4−. Importantly, there is no apparent correlation of $i_{E^{o\prime}}$ to the hydrated diameter of the probes: $Fe(bpy)_2(CN)_2$ is the largest probe and it yields the highest $i_{E^{o\prime}}$ while the next largest, which is $Mo(CN)_8^{4-}$,[48,67] results in the smallest $i_{E^{o\prime}}$. In general, the magnitude of the Faradaic current decreases with increasing ionic charge. However, the sign of the charge influences the extent of pore penetration for at least $Ru(NH_3)_6^{3+}$. If we compare the voltammograms for $Ru(NH_3)_6^{3+}$ and $Fe(bpy)(CN)_4^{2-}$, which have the same hydrated diameters, we find that $i_{E^{o\prime}}$ is much higher for $Ru(NH_3)_6^{3+}$. Moreover, when we started the experiment with $Fe(bpy)_2(CN)_2^+$ and reduced it to the neutral compound, we observed a voltammogram more characteristic of radial than linear diffusion. Since $Fe(bpy)_2(CN)_2^0$ and $Fe(bpy)_2(CN)_2^+$ are essentially identical except for their charge, we infer that ionic charge is most responsible for the enhanced pore exclusion of the oxidized molecule.

From the data given in Figure 3, we conclude that the extent of probe penetration correlates best with the ionic charge of the probe: uncharged molecules penetrate most easily and ions with large negative charges penetrate less easily. This conclusion seems to imply that, at least for molecules of roughly the same size, discrimination is based on chemical characteristics rather than physical size, which would favor smaller probes, or electric field-induced migration, which would favor penetration by more highly charged probes. We conclude that the most hydrophobic molecule, which based on its very low solubility in water is $Fe(bpy)_2(CN)_2$ (~0.2 mM at 25 °C),[68] penetrates the pores most easily and therefore we infer that the pores have hydrophobic interiors. This result is in accord with those of Creager[69] and Majda.[47] Simple chemical intuition leads to the same conclusion. It is curious, however, that the more highly charged positive ion is less excluded than ions with smaller negative charges, even though they have similar solubilities. Since positive ions are usually more highly solvated than negatively charged ions, it is possible that waters of hydration are stripped from the ions prior to their entering the hydrophobic pores.

There are at least two alternative explanations for selective pore penetration. However, since we have no direct or indirect evidence for these hypothesis, we view them as less likely than the ionic-charge model. It is possible that the electrode potential affects the structure of the monolayer, particularly in regions near the templates. This effect might lead to selectivity based on redox potential rather than ionic charge. Potential-dependent structural changes have been observed previously in SAMs, but in aqueous electrolytes the effect is small.[70] Moreover, $Mo(CN)_8^{4-}$ and $Fe(bpy)_2(CN)_2$ have nearly identical redox potentials, but very different electrochemical signatures (parts b and h of Figure 3, respectively), which further indicates there is little or no correlation between redox potential and permeability.

Another possible channel for selective permeation is ligand-enhanced electron transfer. Probe molecules possessing ligands that are soluble in the SAM, such as bipyridine, might be able to exchange electrons with the Au surface without wholly inserting into the pore. If this occurs, then our implicit assumption that there is some correlation between pore size and extent of permeation is not correct. We tend to think contributions to the total current from this process are minor, however, since there is such a large difference in the voltammetry of $Fe(bpy)(CN)_4^{2-}$ and $Fe(bpy)_2(CN)_2$ (Figure 3d,h), which both have ligands that might be expected to insert into the template-induced pores and facilitate electron transfer. Moreover, the voltammetries of $Fe(bpy)_2(CN)_2$ and $Fe(bpy)_2(CN)_2^+$ yield curves characteristic of linear and mixed linear/radial diffusion, respectively, which provides additional evidence against ligand insertion. While this pathway, and others we have not explicitly discussed here, may contribute to selectivity of the pores, we hypothesize that the major factor contributing to pore penetration is the ionic charge of the probe molecule.

Pore Size and Number Density. If we assume there are conditions under which the pores act as independent disk-shaped nanoelectrodes, which is reasonable given voltammetry characteristic of radial diffusion, and that the pores have radii of about 0.5 nm, which is a reasonable estimate of their size given that they selectively admit probe molecules in this size regime (Figure 3),[7] we can calculate the approximate pore number density either using the scan rate at which there is a transition from radial to linear diffusion (parts h and i of Figure 2, for example) or by using eq 1.[57]

$$N = \frac{j}{4nFDC^*r_0} \tag{1}$$

In eq 1, N is the number density of nanoelectrodes, r_0 is their average radius, F is the Faraday constant, D and C^* are the diffusion coefficient and concentration of the probe molecule ($Ru(NH_2)_6^{3+}$), respectively, and n is the number of electrons transferred per probe molecule. Applying this analysis to the data shown in Figure 3a, which is representative of our results, we estimate $N = 10$ nanoelectrodes/μm^2.

Similarly, we can use the scan rate at which there is a transition from radial to linear diffusion to calculate the number density of pores. There is a characteristic interpore distance at which the diffusion layers of individual pores overlap and yield voltammetry characteristic of linear diffusion: this transitional behavior is shown in Figure 2g–i. To make this calculation, we invoke theory developed by Amatore et al.[60] and experimental confirmation by Sabatani and Rubinstein,[55] which are summarized by eq 2, where d is the distance between pores, R is the gas constant, T is the absolute temperature,

(63) Licht, S.; Cammarata, V.; Wrighton, M. S. *J. Phys. Chem.* **1990**, *94*, 6133.

(64) Bard, A. J.; Crayston, J. A.; Kittlesen, G. P.; Shea, T. V.; Wrighton, M. S. *Anal. Chem.* **1986**, *58*, 2321.

(64) Bockris, J. O.; Reddy, A. K. N. In *Modern Electrochemistry*; Plenum: New York, 1970; p 380.

(65) Saji, T.; Maruyama, Y.; Aoyagui, S. *J. Electroanal. Chem.* **1978**, *86*, 219.

(66) Odashima, K.; Kotato, M.; Sugawara, M.; Umezawa, Y. *Anal. Chem.* **1993**, *65*, 927.

(67) Blandamer, M. J.; Burgess, J.; McGowan, J. C. *J. Chem. Soc., Dalton Trans.* **1980**, *4*, 616.

(68) Groat, K. A.; Creager, S. E. *Langmuir* **1993**, *9*, 3668.

(69) Anderson, M. R.; Gatin, M. *Langmuir* **1994**, *10*, 1683.

v_{max} is the scan rate at which the transition from radial to linear diffusion occurs, and the rest of the variables have the meanings defined for eq 1.[71]

$$d \cong \sqrt{\frac{(DRT/Fv_{max})^{1/2} r_0}{4.44}} \quad (2)$$

If we again assume r_0 to be about 0.5 nm and take v_{max} to be 1 mV/s (Figure 2i) then $d = 123$ nm, which corresponds to a pore density of about 65 nanoelectrodes/μm^2. This compares with the estimate of 10 nano-electrodes/μm^2 determined from the magnitude of the limiting current obtained. This level of agreement is gratifying given that the two analyses are based on different experimental bases, were obtained using electrodes prepared on different substrates on different days, and that there is a significant degree of arbitrariness in picking v_{max}.

Monolayer Selectivity in Binary Mixtures of Redox Molecules. Since our goal is to show that template-induced defects discriminate between molecules having different chemical and physical characteristics, we exposed a suitably modified electrode to electrolyte solutions containing a mixture of two of the probe molecules discussed in the previous section. The results of this study show that the voltammetry of the two compounds is a simple sum of the single-component voltammetry, which unambiguously demonstrates selectivity and illustrates the important result that the two probe molecules do not interfere with each other.

We chose to compare $Ru(NH_3)_6^{3+}$ and $Fe(bpy)_2(CN)_2$ first, because they have the best-defined voltammetry. The results of this study are shown in Figure 5. Parts a and b of Figure 5 show the voltammetry of single-component solutions of $Ru(NH_3)_6^{3+}$ and $Fe(bpy)_2(CN)_2$, respectively. These data are essentially identical to those shown in parts g and h of Figure 3 except they were obtained using a different electrode on a different day: the slight differences in the voltammetry shown in these two pairs of figures is typical of the day-to-day variation we observe in the voltammetry of nominally identical SAM-coated electrodes.[72] As discussed earlier, we find that the voltammetry of $Ru(NH_3)_6^{3+}$ (Figure 5a) is characteristic of nearly pure radial diffusion, while the voltammetry of $Fe(bpy)_2(CN)_2$ is more characteristic of linear diffusion. Parts c, e, f, and g of Figure 5 are control experiments that indicate that the characteristics of the nanoporous SAM are not changed by the preceding voltammetric experiments.

The critical voltammogram in this data set is shown in Figure 5d. Both probe molecules are present in the solution simultaneously in this experiment. There are some slight differences between the voltammetric waves resulting from the binary and single-component experiments, but they are minor. The more important observation is that $i_{E^{o\prime}}$, normalized for the differences in C^* and D, is higher for $Fe(bpy)_2(CN)_2$ than it is for $Ru(NH_3)_6^{3+}$ and that the shapes indicate mixed radial/linear diffusion for the former, but nearly pure radial diffusion for the latter. From these data, we conclude that $Fe(bpy)_2(CN)_2$ is able to access more template-induced defect sites than

(70) This expression follows directly from ref 60 and is given explicitly in ref 55 (eq 1 and eq 2). We have used the approximation that $1 - \theta = r_0^2/(d/2)^2$, which is appropriate when $(1 - \theta) < 0.1$ (Finklea, H. O.; Snider, D. A.; Fedyk, J.; Sabatani, E.; Gafni, Y.; Rubinstein, I. *Langmuir* **1993**, *9*, 3660).

(71) The day-to-day variation in the response of the nanoporous SAMs is illustrated by comparing Figures 2d, 3a, 5a, 8a, and 9a, which were obtained using nominally identical electrodes. Figure 1d is somewhat different from the others because it was removed from the 4-HTP/C16-SH solution periodically so that Figure 1a−1c could be obtained.
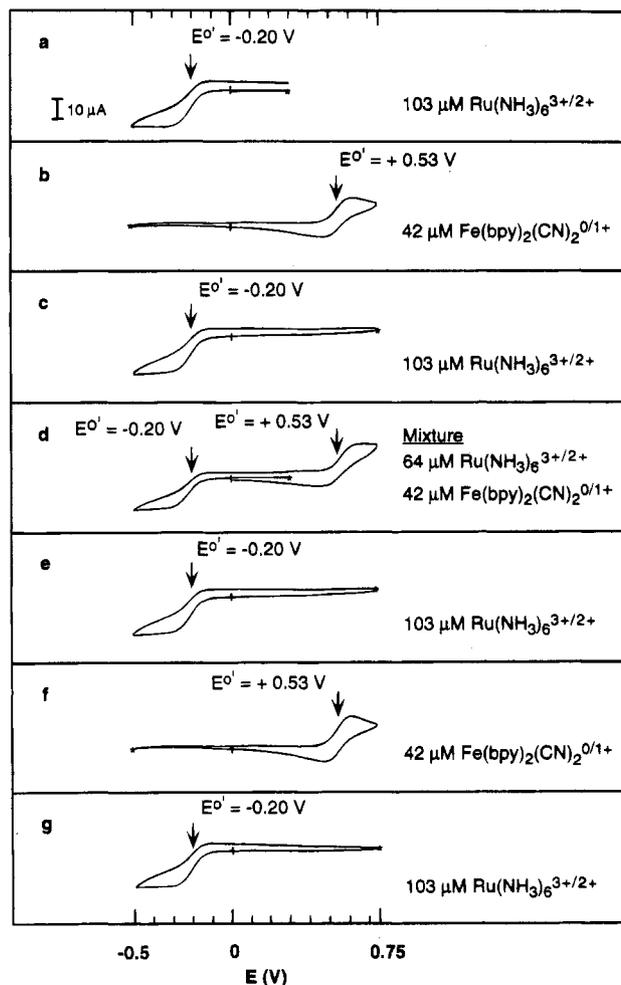

Figure 5. Cyclic voltammograms of (a−c, e−g) single-component redox-probe solutions and (d) a binary mixture. A single nanoporous-SAM electrode was used to obtain the data. The probe molecules, their concentrations, and their $E^{o\prime}$ values measured on naked Au electrodes are indicated in each frame. The elecrolyte was 0.2 M KF. The scan rate was 0.1 V/s in all cases. The asterisks indicate the point where the scan was initiated.

$Ru(NH_3)_6^{3+}$. The differences in the voltammetry are not great in this example, but other pairs of probes result in more striking contrasts (*vide infra*).

Figure 6 shows the differences in electrode selectivity for a different pair of molecules: $Fe(bpy)_2(CN)_2$ and $Fe(bpy)(CN)_4^{2-}$. This pair is structurally similar, but the probes differ greatly in their ionic charges. The voltammograms on the left side of Figure 6 are control experiments that show the electrochemical response of the modified electrode is stable throughout the duration of this experiment. These experiments allow us to directly compare the voltammetry on the right side of Figure 6.

Figure 6b is a voltammogram of a dilute solution of $Fe(bpy)_2(CN)_2$ obtained at a 4-HTP/C_{16}SH = 5-modified electrode. The data indicate considerable penetration by the probe. Figure 6d shows analogous data for $Fe(bpy)(CN)_4^{2-}$, but here the degree of penetration is much smaller: little current is observed at $E^{o\prime}$, although control experiments indicate that the current rise at more positive potentials is due to probe penetration. The important result, however, is shown in Figure 6f. This is a voltammogram of a nearly equimolar solution of $Fe(bpy)_2(CN)_2$ and $Fe(bpy)(CN)_4^{2-}$. At a macroscopic, nonselective Au electrode we observe two distinct peaks of approximately equal height (when corrected for differences in C^* and D) separated by about 200 mV. The presence of two peaks
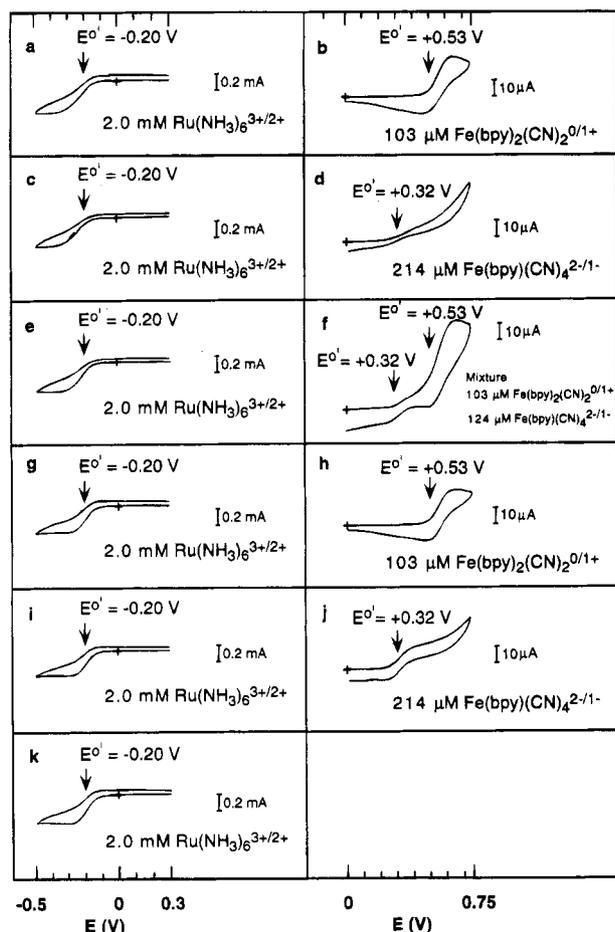
Figure 6. Cyclic voltammograms of (a–e, g–k) single-component redox-probe solutions and (f) a binary mixture. A single nanoporous-SAM electrode was used to obtain the data. The probe molecules, their concentrations, and their $E^{o\prime}$ values measured on naked Au electrodes are indicated in each frame. The electrolyte concentration was 0.2 M KF and the scan rate was 0.1 V/s.
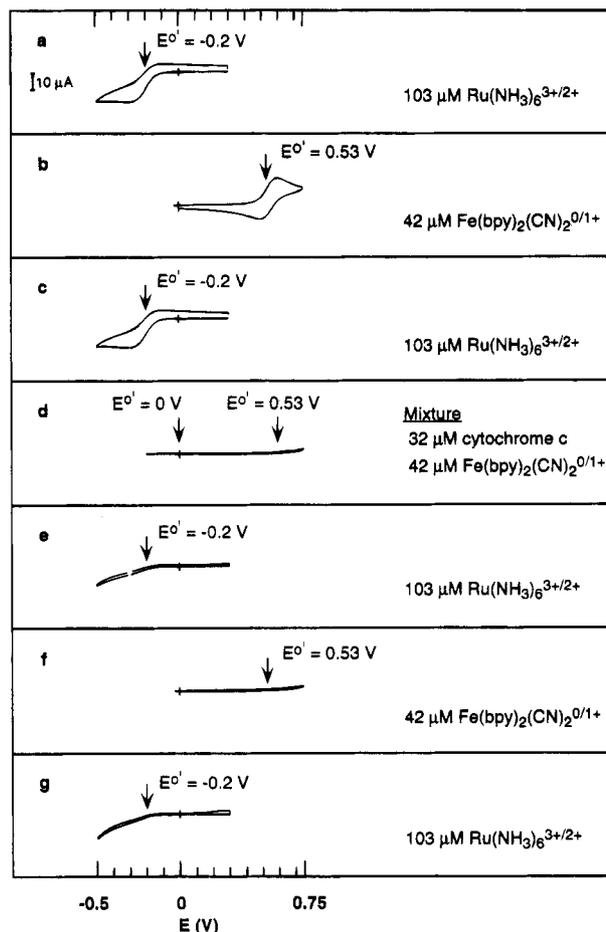
Figure 7. Cyclic voltammograms of (a–c, e–g) single-component redox-probe solutions and (d) a binary mixture. A single nanoporous-SAM electrode was used to obtain the data. The probe molecules, their concentrations, and their $E^{o\prime}$ values measured on naked Au electrodes are indicated in each frame. The scan rate was 0.1 V/s and the electrolyte was 0.2 M KF. The current scale shown in (a) was used for all frames.

at the same potentials found for the individual, unmixed redox probes confirms that $Fe(bpy)_2(CN)_2$ and $Fe(bpy)(CN)_4{}^{2-}$ do not undergo ligand change. At the nanoporous SAM-modified electrode, however, we observe relatively little current from the charged probe compared with the uncharged molecule. This result unambiguously demonstrates the selective nature of the modified electrode, and it also provides dramatic evidence that the nanoporous defect sites are of molecular dimensions. In addition, it shows that the voltammetry of mixed redox probes is approximately the sum of the individual probes. This is an anticipated but important finding, since it proves that the probes interact with the pores independent of one another. Although we note little difference between parts b and h of Figure 6, or between any of the $Ru(NH_3)_6{}^{3+}$ voltammetry shown on the left side of Figure 6, there is a significant difference between the two voltammograms associated with $Fe(bpy)(CN)_4{}^{2-}$ (parts d and j of Figure 6). This observation demonstrates that very small changes in the structure of the monolayer, which in this case are too small to detect using $Ru(NH_3)_6{}^{3+}$ (compare parts a and k of Figure 6), can significantly affect the electrode response for other probes.

Figure 7 shows voltammetry for a third pair of probe molecules: cytochrome c and $Fe(bpy)_2(CN)_2$. The voltammetry for $Ru(NH_3)_6{}^{3+}$ in parts a and c of Figure 7 and for $Fe(bpy)_2(CN)_2$ in Figure 7b confirm the integrity of the modified electrode. Figure 7d shows the voltammetry of a mixture of cytochrome c and $Fe(bpy)_2(CN)_2$. We observe

no Faradaic current attributable to cytochrome c; we originally attributed this directly to the large size of this probe. When we checked the voltammetry of $Ru(NH_3)_6{}^{3+}$ (Figure 7e,g) and $Fe(bpy)_2(CN)_2$ (Figure 7f), however, we observe greatly suppressed Faradaic and capacitive currents. We attribute this surprising result to irreversible adsorption of cytochrome c either in the pores or possibly over the entire SAM surface. We are continuing to study cytochrome c and other large molecules to better understand this interesting result.

Effect of Electrolyte Concentration and Type on the Voltammetry of $Ru(NH_3)_6{}^{3+}$. Figure 8 illustrates the effect of different KF electrolyte concentrations on the voltammetry of $Ru(NH_3)_6{}^{3+}$ at a 4-HTP/C$_{16}$SH-modified electrode. We chose to use KF as the electrolyte in this part of the study because F$^-$ does not interact specifically with Au electrodes. The voltammograms on the left side of Figure 8 are control experiments that show the voltammetry of $Ru(NH_3)_6{}^{3+}$ in different electrolyte concentrations does not greatly affect the structural integrity of the nanoporous SAM, although minor changes do occur (compare parts a and m of Figure 8). There are two interesting results that we obtain from these data.

First, the limiting current and general shape of the voltammograms are a function of the electrolyte. At very high electrolyte concentration (Figure 8b) the limiting current is lowest. It is tempting to rationalize this observation in terms of mass transfer effects: at high
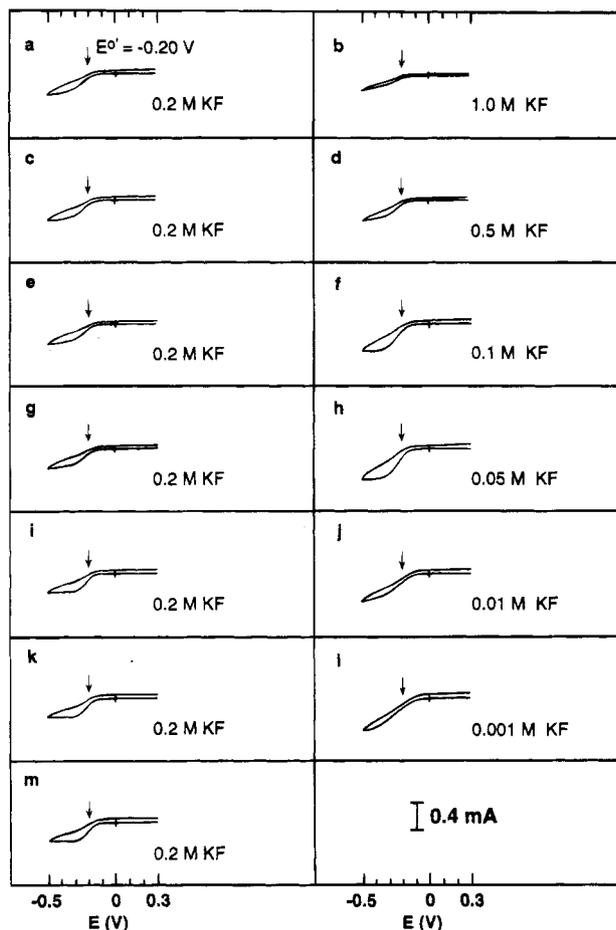
Figure 8. Cyclic voltammograms of 2 mM $Ru(NH_3)_6^{3+}$ solution as a function of the KF electrolyte concentration. All data were obtained using the same nanoporous-SAM electrode. The $E^{o\prime}$ value for $Ru(NH_3)_6^{3+}$ measured on a naked Au electrode is indicated in each frame. The electrolyte concentrations are also indicated in each frame. The scan rate was 0.1 V/s.

electrolyte concentrations the probe moves only by diffusion and convection, but at low concentrations migration also contributes. However, it does not seem physically reasonable that a change in electrolyte concentration from 1.0 M (Figure 8b) to 0.5 M (Figure 8d) would lead to such a dramatic change in the rate of mass transport. Therefore, we conclude that the size and shape of the pores must be electrolyte-concentration dependent. If one considers the common phenomenon of "salting-out", the data on the right side of Figure 8 are self-consistent.[73,74] It is well-known that electrolytes decrease the solubility of organic substances, particularly biological molecules, in water and that the effect is only appreciable at very high electrolyte concentrations. Differences in solubility are related to the magnitude and sign of the ionic charge and the ionic radius. In Figure 8b, therefore, we speculate that the nanoporous SAM has precipitated or collapsed in regions around the defect sites, thereby excluding probe molecules and lowering the Faradaic current. As the electrolyte concentration is lowered, the pores open to provide better access to the probe and the current increases. We envision a transition from the situation depicted in part b of Chart 4 to that shown in part a as the electrolyte concentration is lowered. At least in bulk phases, electrolyte effects on the solubility of hydrocarbons

dissolved in water only occur at concentrations greater that about 0.3 M.[74] If we extrapolate this result to the monolayers discussed here, then we expect a gradual increase in Faradaic current until the electrolyte concentration falls below 0.3 M and then we anticipate little further change. Indeed, we observe this trend (parts b, d, f, and h of Figure 8). However, at even lower electrolyte concentrations (parts j and l of Figure 8) the shape of the voltammograms begin to change in a way that strongly suggests a very high solution resistance. We also note in passing that the magnitude of the electrode capacitance increases with decreasing electrolyte concentration.[75] This result is consistent with our hypothesis that the framework collapses around the pores at high electrolyte concentration.

An alternative to this salting-out hypothesis involves a competition for pores between the redox probe molecule and K^+. In this case K^+ would compete most effectively for the pores at high concentration, with the result that the Faradaic current would decrease and the interfacial capacitance would increase as the concentration of K^+ in the solution increased. Although we do observe a decrease in Faradaic current at a high K^+ concentration, the capacitive current decreases, rendering this hypothesis less likely than salt-induced collapse of the SAM.

To further investigate the effects of the electrolyte on the electrochemical response of nanoporous SAMs, we examined the voltammetry of $Ru(NH_3)_6^{3+}$ in 0.2 M aqueous solutions of KF, KCl, KNO_3, and K_2SO_4 and an electrolyte solution consisting of 0.1 M K_2HPO_4 plus 0.1 M KH_2PO_4. We used the 3 × 5 matrix of voltammograms on the left side of Figure 9 as a control to ensure that the single SAM-modified electrode that was used to collect all 27 voltammograms did not change significantly during the course of the experiments. We conducted the experiments in groups of three voltammograms to ensure that the results were reproducible. For example, the first set of experiments were conducted at scan rates of 100, 10, and then 100 mV/s in 0.2 M KF. The electrode was rinsed with water and then we obtained another set of three voltammograms in a 0.2 M KCl electrolyte solution at the same three scan rates. We often noticed that the first scan in a different electrolyte resulted in voltammograms that were uncharacteristic of those that had been recorded at slow scan rates (10 mV/s) once. This effect, the origin of which is not clear at the present time, is most apparent in the following pairs of voltammograms: parts j and l, p and r, and v and x of Figure 9.

The results indicate that the extent of pore penetration by $Ru(NH_3)_6^{3+}$ is similar in the monovalent-halide and nitrate-containing electrolyte solutions. In contrast, the limiting currents observed for the divalent and trivalent anions is suppressed to roughly half that of the monovalent ions. For now, we ascribe these observations to the same salting-out, or SAM-precipitation, phenomenon discussed earlier, except here it is exacerbated by the more highly charged anions rather than increased electrolyte concentration only. Note, however, that the total ionic strength of the electrolyte solutions containing the multivalent anions is higher than that in the solutions containing monovalent anions.

Conclusions

In this paper, we have confirmed and expanded upon our earlier finding that mixed monolayers of organomer-

(72) Bockris, J. O.; Reddy, A. K. N. In *Modern Electrochemistry*; Plenum: New York, 1970; pp 158–159.

(73) Tanford, C. In *The Hydrophobic Effect: Formation of Micelles and Biological Membranes*; Wiley: New York, 1980; p 11.

(74) Bard, A. J.; Faulkner, L. R. In *Electrochemical Methods*; Wiley: New York, 1980; pp 500–515.

(75) Allen, P. M.; Hill, H. A. O.; Walton, N. J. *J. Electroanal. Chem.* **1984**, *69*, 178.
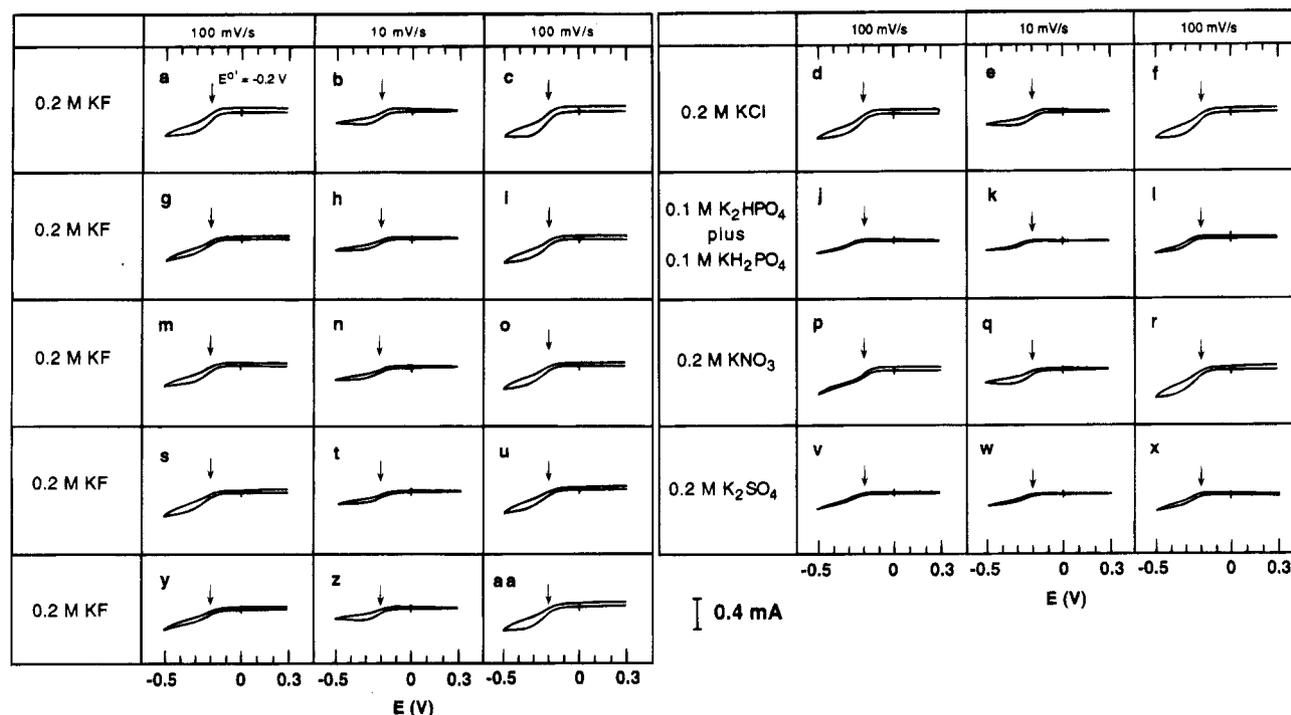
Figure 9. Cyclic voltammetry of a 2 mM $Ru(NH_3)_6^{3+}$ solution in the indicated electrolyte solution. Data were obtained using a single nanoporous-SAM electrode. The $E^{o\prime}$ value of $Ru(NH_3)_6^{3+}$ measured at a naked Au electrode in 0.2 M KF is indicated by an arrow in each frame. The current scale is indicated at the bottom of the figure.

captans can act as nanoporous organic surfaces. The nanoporous SAMs are easily and reproducibly formed, and they are stable under a broad range of conditions. Depending on the fabrication conditions, the SAMs may contain widely spaced pores of molecular dimension.

Our results indicate that in favorable cases the SAM-modified electrodes are able to discriminate between probe molecules with different physical and chemical characteristics. For molecules that vary in size by only a few angstroms, selectivity is dominated by the probe's ionic charge. Since the electrically neutral probe molecule penetrates most easily, we hypothesize that the interiors of the pores are hydrophobic. We have also shown that

the degree of pore selectivity can be affected by the type and concentration of the electrolyte, which suggests there is an important interaction between SAMs and ionic solutions.